fortune Journals

Research Article

FORTUNE JOURNAL OF HEALTH SCIENCES

ISSN: 2644-2906

ERK5 Mediates Metastatic Colonization and Remodeling of The Tumor and Tumor-Immune Microenvironment and Immunotherapy Response

Mariska Miranda[1], Oishee Chatterjee[1], Esdy Rozali[1], Sujitha Jeya[2], Sarra Mestiri[2], Mariam Al-Muftah[2] and Fares Al-Ejeh[*,2,3,4]

Abstract

ERK5 plays diverse roles in cancer progression including proliferation, epithelial-mesenchymal transition, and metastasis. We recently reported that different subcellular localizations of active phosphorylated-ERK5 (pERK5) in cancer cell lines and patient tumors associated with different molecular features and survival outcomes in breast cancer. We also showed that shorter isoforms of ERK5 play an important role in the nucleocytoplasmic shuttling of pERK5. In this study, we used in vitro and in vivo models to further understand the role of ERK5 in colonizing distant metastatic sites, and how ERK5 modulates pathways involved in the tumor and the immune microenvironment. For clinical context, we used the TCGA pan-cancer data to interrogate the correlation between pathways identified from our experimental studies and the expression of ERK5 and ERK5 isoforms in patients. We found that ERK5 is essential for colonizing metastatic sites in mice by mediating cell migration and invasion, remodeling the extracellular matrix (ECM) and regulating oncogenic and immune signaling pathways. The situation of ERK5 as a key protein in the crossroads between growth factor signaling, cytokine signaling, ECM remodeling and other functions was supported by strong correlations in the TCGA pan-cancer data between those pathways and the expression of ERK5 and ERK5 isoforms. Consequently, we validated our findings experimentally where we show that *ERK5*-depleted tumors in mice have denser collagen fibers suggesting a defect in ECM degradation and remodeling, have higher CD8 and CD4 T-cell infiltration and lower expression of PD-L1, and although they grow similarly to ERK5 wild-type tumors, *ERK5*-depleted were significantly sensitized to anti-PD1 immunotherapy. Our study supports a major role for ERK5 in the remodeling of the tumor and tumor-immune microenvironment that drives aggressive behavior thus could be a potential target for rationalized combination therapy.

Keywords: ERK5, extracellular matrix remodeling, tumor microenvironment, tumor-immune microenvironment, immunotherapy

Introduction

Breast cancer (BC) is the most diagnosed cancer worldwide and the leading cause of cancer deaths among women (1). Triple negative cancer (TNBC) accounts for 15 to 20% of all BC and is considered as the most aggressive subtype (2). Compared to other subtypes, TNBC is characterized by a higher recurrence and metastatic rates, poorer prognosis and lower survival rates (3, 4). Indeed, more than one-third of TNBC patients can develop distant

Affiliation:

[1]Cancer Program, QIMR Berghofer Medical Research Institute, Herston, Australia

[2]Qatar Biomedical Research Institute (QBRI) – Hamad Bin Khalifa University (HBKU), Qatar Foundation, Doha, Qatar

[3]College of Health and Life Sciences (CHLS) - Hamad Bin Khalifa University (HBKU), Qatar Foundation, Doha, Qatar

[4]Previously at Cancer Program, QIMR Berghofer Medical Research Institute, Herston, Australia

***Corresponding author:**
Fares Al-Ejeh, College of Health and Life Sciences (CHLS) - Hamad Bin Khalifa University (HBKU), Qatar Foundation, Doha, Qatar.

Citation: Mariska Miranda, Oishee Chatterjee, Esdy Rozali, Sujitha Jeya, Sarra Mestiri, Mariam Al-Muftah and Fares Al-Ejeh. ERK5 Mediates Metastatic Colonization and Remodeling of The Tumor and Tumor-Immune Microenvironment and Immunotherapy Response. Fortune Journal of Health Sciences 8 (2025): 491-502.

Received: May 08, 2025
Accepted: May 15, 2025
Published: June 09, 2025

metastasis in the third year after diagnosis (5). Therefore, understanding the molecular mechanisms and signaling pathways involved in BC metastasis is an urgent need to improve treatment outcomes and develop novel and effective therapeutic strategies. Extracellular signal-regulated kinase 5 (ERK5) is a member of the mitogen-activated protein kinases (MAPK) family and is encoded by the MAPK7 gene. ERK5 is distinct from other MAPKs family members given its large structure, its unique C-terminal region that can regulate the transcriptional activity of several target proteins and it can be activated by autophosphorylation (6). The dual-function protein kinase and transcriptional regulator functions implicate ERK5 in various oncogenic processes including proliferation, epithelial-mesenchymal transition (EMT), drug resistance and metastasis (6, 7). In our previous study (8), we identified ERK5 isoform-3, a naturally occurring splice variant lacking the C-terminal transcriptional domain, which retained phosphorylated ERK5 (pERK5) in the cytoplasm and promoted EMT, cell migration, and therapy resistance. We demonstrated that co-expression of isoform-1 (full-length) and isoform-3 was associated with a mesenchymal phenotype and poor prognosis across multiple cancer types, particularly TNBC. This led us to hypothesize that ERK5 differentially regulates tumor progression through both cell-autonomous and microenvironmental mechanisms. In this follow-up study, we explored how ERK5 expression affects metastatic colonization, modulation of the tumor immune microenvironment (TIME), and response to immune checkpoint blockade. Our approach integrates metastasis mouse models, targeted profiling, assessment of tumors in mice after silencing ERK5, and the TCGA pan-cancer dataset to evaluate the oncogenic and immune pathways from experimental studies in the clinical context, particularly attempting to dissect ERK5 isoform-specific functions and therapeutic implications.

Results

ERK5 is required for efficient metastatic colonization and survival in the lung

We previously showed that *ERK5* depletion via stable expression of shRNAs had no effect on primary tumor formation or growth but inhibited spontaneous metastasis in two TNBC models; MDA-MB-231 (MDA231) human xenograft and the 4T1.2 syngeneic mouse models (8). Here we used intravenous cell delivery to bypass the intravasation step of metastasis to test the cell ability to colonize and expand as metastases in the lungs. In this experimental metastasis model, *ERK5* depletion significantly protected against lung metastases over the 130 days of observation (**Figure 1A&B**), suggesting that these cells could not migrate into and colonize the lungs to expand into metastases. We addressed this possibility directly by additional experimental metastases studies and collecting lungs from mice immediately (less than 1 hour from injection) or on days 1, 3 and 6 post injection. Histological analysis revealed that despite equivalent delivery of cells to all mice (**Figure 1C**), *ERK5*-depleted cells showed lower proliferation (Ki67) and increased apoptosis (Apoptag) during early colonization (**Figure 1D&E**). We confirmed these results in a second experiment with the same design and included vimentin IHC staining to better track cancer cells (**Figure S1**). The results from this experimental metastasis model suggest that ERK5 supports cell migration and extravasation into the tissue of a distant site and the ability to expand and establish metastases. To explore the signaling consequences of *ERK5*-depletion, we assessed cell motility under basal and stimulated conditions (EGF, TNF, and TGF-β). *ERK5* depletion significantly impaired migration across all stimuli to similar levels as the ERK5 inhibitor (XMD8-92) (**Figure 2A&B**). Then we performed transcriptomic (NanoString PanCancer Pathways panel) and proteomic (Proteome Profiler™ Antibody Arrays) profiling of *ERK5*-depleted MDA-MB-231 cells (**Table S1**). Pathway analysis revealed deregulation of growth factor receptor signaling, ECM remodeling, cytokine signaling, and inflammatory pathways (**Figure 2C&D**; **Tabel S1**). In line with the frequent alterations of ECM-remodeling factors that play a role metastasis-related processes such as cell migration, invasion and adhesion, we confirmed the reduction of secretion and activity of various proteases in culture media from *ERK5*-depleted or XMD8-92 treated cells (**Figure S2**).

ERK5 mediates remodeling the tumor microenvironment

Before further exploration, we wanted to test our lab-based hits and pathways for clinical relevance, and to gain insight into the potential roles of ERK5 isoforms in our observations. To this end, we used the same TCGA pan-cancer dataset of 8,947 patients where we included the expression of total ERK5 (gene-level expression) and the expression of ERK5 transcript variants (8). This data includes transcripts that encode full length ERK5 (isoform-1), the C-terminal loss transcript variant (isoform-3), the N-terminal loss transcript variant (isoform-2), and the co-expression of isoform-3 and isoform-1 which associated with high epithelial-to-mesenchymal transition (EMT) and poor patient survival (8). The pan-cancer dataset was supplemented with the RNA expression of all the significant hits we found from our profiling, previously published gene programs and canonical targetable pathways (collectively called GPs here) and 1378 PARADIGM-inferred pathways expressed as z-score for ssGSEA - single sample gene set enrichment analysis (9), and estimation of the proportion of tumor-infiltrating immune cell types based on two different RNA-seq deconvolution methods; CIBERSORT (10) and MIXTURE (11). First, we investigated the expression of 175 RNAs and proteins that

Miranda M, et al., Fortune J Health Sci 2025
DOI:10.26502/fjhs.299

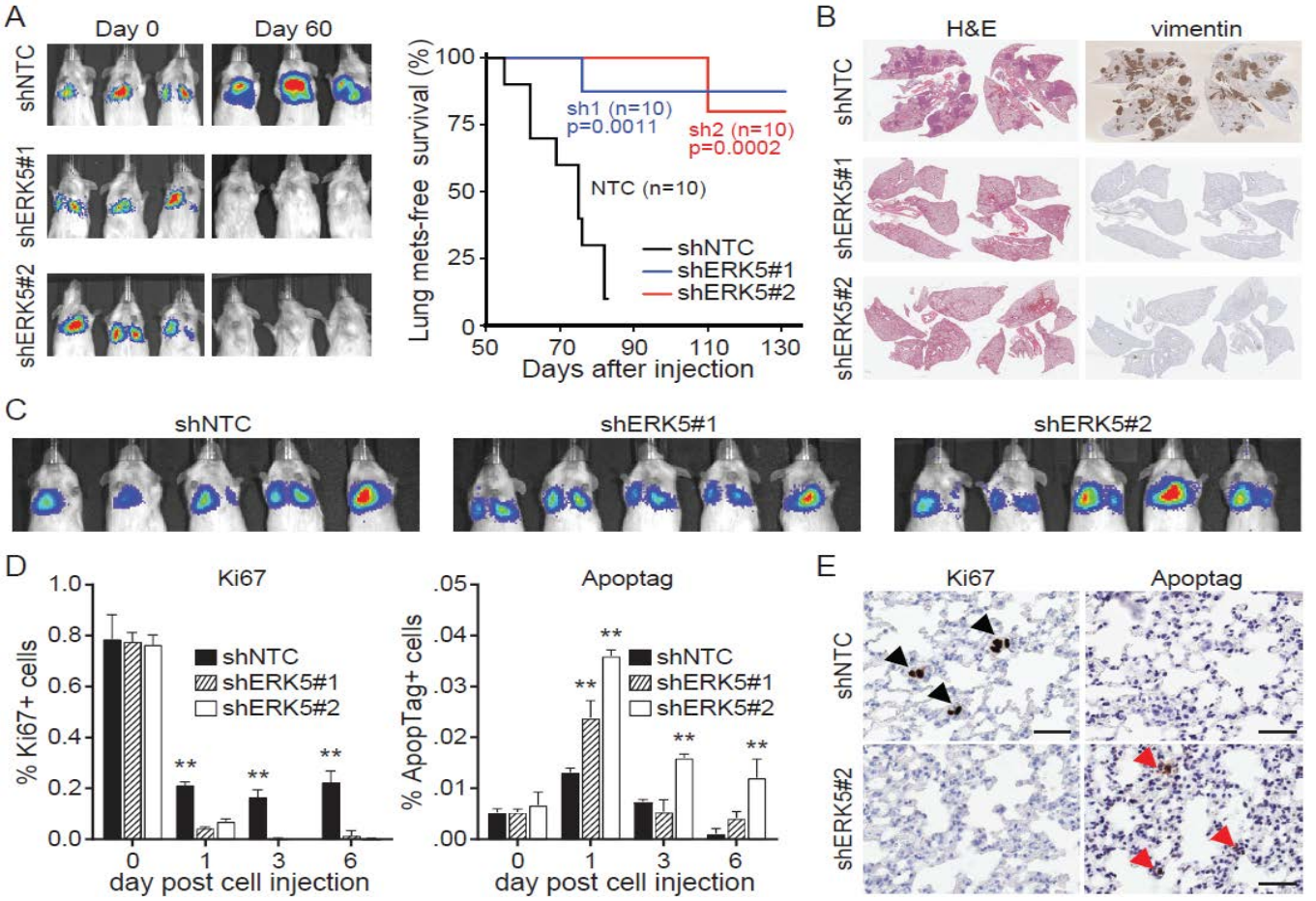

Figure 1: ERK5 is essential for metastatic colonization. (**A & B**) Long-term follow up of lung metastases after tail vein injection of MDA-MB-231 control cells (non-target shRNA control shNTC) or cells with *ERK5* depletion (shERK5#1 and shERK5#2), followed by immediate imaging to confirm delivery then regular weekly imaging. Lung metastasis-free survival was compared by log-rank (n = 10 per group from two independent experiments). Representative H&E and vimentin staining on lungs are shown at sacrifice or at 20 weeks after intravenous injection for the *ERK5*-depleted groups. (**C - E**) Short term (0 - 6 days) follow up of lung metastasis after intravenous injection of MDA-MB-231 cells. After immediate confirmation of cell delivery using live animal imaging (panel C), IHC was used to detect proliferation (Ki67) and cell death (ApopTag) immediately after imaging and on days 1, 3, 6, and staining was quantified using IHC Profiler. Data shown is the mean ± SEM (n = 3/time point/group; repeat experiment shown in Figure S1). * P<0.05, ** P<0.01 and *** P<0.001; two-way ANOVA with Dunnett multiple comparison test. Representative images (panel E, scale bar = 40 mm) of Ki67 and ApopTag IHC on lungs at 72 hours post intravenous injection of cells.

were significantly affected by ERK5 depletion or inhibition. Of those hits, 110 (63%) significantly correlated with the expression of total ERK5 or with isoforms 1 or 3, or the co-expression of these two isoforms in the TCGA pan-cancer data in the same direction as our lab results (**Figure 3A**, Table S3). Pathway analysis (KEGG pathways and GO biological processes) based on the 110 RNAs reproduced the same results from analyzing all the 175 hits from the lab profiling (Table S3).

The top KEGG pathways from the lab profiles and those replicating in the TCGA dataset were highly similar including focal adhesion, EGFR TKi resistance, PI3K-Akt and MAPK signaling pathways (Figure S3A&B). The top GO biological processes were also similar and notably included ECM disassembly, and collagen metabolic and catabolic processes (Figure S3C&D). To broaden our confirmation of pathways relating to the expression of ERK5 or its isoforms in the TCGA pan-cancer dataset, we correlated the expression of ERK5 and ERK5 isoforms expression with gene programs and canonical pathways (GPs) scores in dataset. The expression of total ERK5 or isoform-3 and/or isoform-1 had strong positive correlation with oncogenic signaling pathways and GP4 ECM/MES (mesenchymal) program, but negative correlation with many immune-related programs and pathways (**Figure 3B&C**, Figure S4, Table S4). These two features, oncogenic signaling/ECM and

Citation: Mariska Miranda, Oishee Chatterjee, Esdy Rozali, Sujitha Jeya, Sarra Mestiri, Mariam Al-Muftah and Fares Al-Ejeh. ERK5 Mediates Metastatic Colonization and Remodeling of The Tumor and Tumor-Immune Microenvironment and Immunotherapy Response. Fortune Journal of Health Sciences. 8 (2025): 491-502.

Miranda M, et al., Fortune J Health Sci 2025
DOI:10.26502/fjhs.299

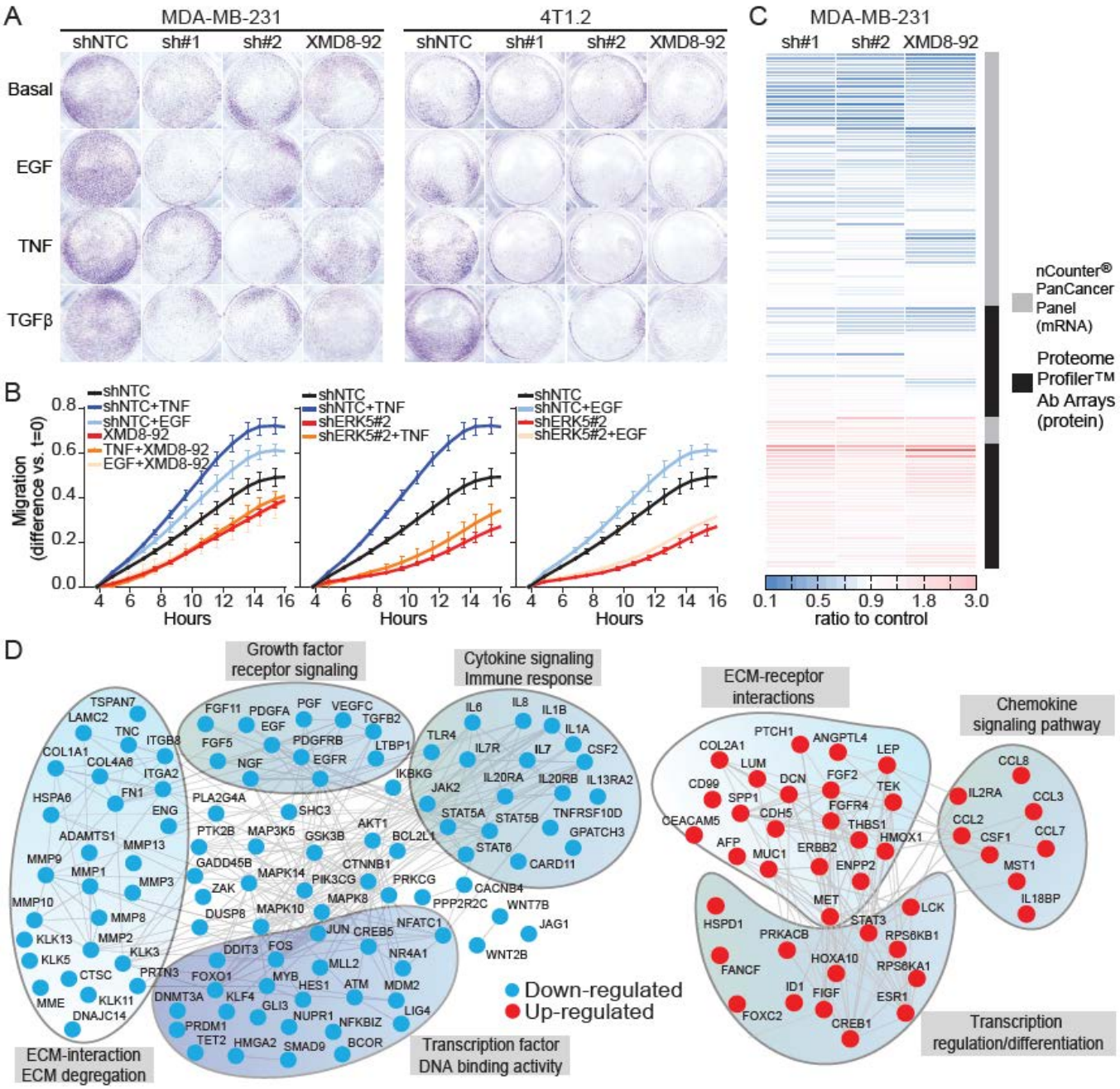

Figure 2: ERK5 depletion inhibits cell migration and modulates related pathways. (**A&B**) Conventional endpoint and real-time (xCELLigence system - CIM-Plate®) Transwell cell migration assays of control (shNTC) and *ERK5*-depeleted cells. The human MDA-MB-231 cells and the mouse 4T1.2 cells were subjected to cell migration assays in the absence (basal condition) or presence of growth factors (200 ng/mL EGF, 100 ng/mL TNF or 100 ng/mL TGFb), or the ERK5 inhibitor XMD8-92. Representative data are shown from three independent assays for both cell lines in the conventional assays, and real-time migration assays using the with control and *ERK5*-depeleted 4T1.2. All curves were significantly different from shNTC control cells (one-way ANOVA on the area under the curves, $P < 0.05$ at least). (**C**) Panel profiling of the effect of ERK5 depletion or the ERK5 inhibitor XMD8-92 in MDA-MB-231 cells with the nCounter® PanCancer Pathways Panel (mRNA, marked grey) and the Proteome Profiler™ Antibody Arrays (the phospho-kinase, XL-oncology, and protease antibody arrays, marked black). The heatmap is the ratio of expression in comparison to control (shNTC) MDA-MB-231 cells (full data in Table S1). (**D**) Network analysis using the STRING-database of the genes and proteins that were commonly affected by *ERK5*-depletion or inhibition with XMD8-92. Targets which were downregulated with *ERK5*-depletion or inhibition appear in blue, while upregulated targets are in red. The list of all enriched KEGG and Reactome Pathways is detailed in Table S1 – Pathways.

Citation: Mariska Miranda, Oishee Chatterjee, Esdy Rozali, Sujitha Jeya, Sarra Mestiri, Mariam Al-Muftah and Fares Al-Ejeh. ERK5 Mediates Metastatic Colonization and Remodeling of The Tumor and Tumor-Immune Microenvironment and Immunotherapy Response. Fortune Journal of Health Sciences. 8 (2025): 491-502.

Miranda M, et al., Fortune J Health Sci 2025
DOI:10.26502/fjhs.299

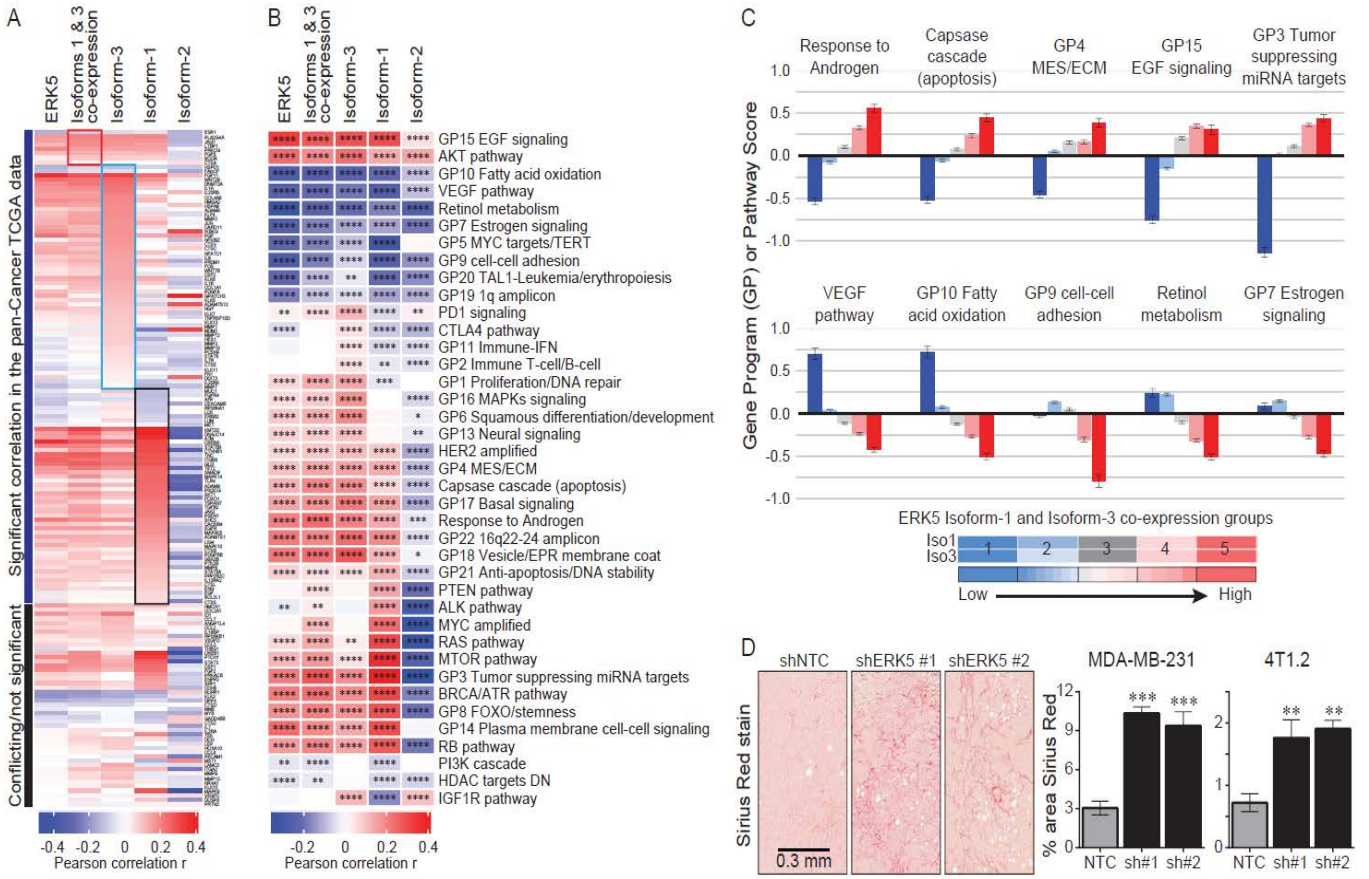

Figure 3: ERK5 modulates oncogenic signaling and the tumor microenvironment. (**A**) The 175 genes and proteins affected by *ERK5*-depletion or inhibition were evaluated in the TCGA pan-cancer dataset for correlation with total ERK5 and ERK5 isoforms expression. The heatmap depicts Pearson correlation r and marking regions where drivers of correlations can be attributed to the co-expression of isoforms 3 and 1 (red box), isoform-3 (blue box) or isoform-1 (black box). The heatmap data are in Table S3 and pathway analysis of the 110 genes in agreement with our profiling is in Figure 3S. (**B**) Correlation between the gene programs and canonical pathways (GPs) in the TCGA pan-cancer dataset and the expression of ERK5 and ERK5 isoforms in the same dataset. Heatmap depicts Pearson correlation r and asterisks mark significant correlations. The heatmap data are in Table S4. (**C**) Selected GPs from panel B were plotted to show top pathways driven by the co-expression of ERK5 isoforms 3 and 1. Refer to Figure S4 for the full list of pathways including those driven by different ERK5 isoforms. (**D**) Sirius Red staining for collagen in MDA-MB-231 and 4T1.2 tumors. Images shown are at 8x magnification (scale bar = 0.3 mm). Bar graphs summarize the quantification (mean ± SEM, n = 3) using IHC Profiler (** P<0.01, *** P<0.001 one-way ANOVA).

immune programs, were also observed when our analysis of the TCGA pan-cancer dataset was further generalized to the 1378 ssGSEA pathways (Figure S5, Table S5). Together, these results strongly support a role for ERK5 and its isoforms as key orchestrators of response to environmental stimuli through diverse signaling pathways and potentially drive structural tumor adaptation. Consequently, for the ECM-related pathway changes, we investigated collagen fibers in our control and *ERK5*-depleted tumors. As shown in **Figure 3D**, MDA-MB-231 and 4T1.2 tumors with *ERK5*-depletion had significantly higher collagen fibers compared to controls supporting the ECM degradation/remodeling is defected in those tumors and could explain their reduced metastatic potential.

ERK5 is implicated in remodeling the tumor immune microenvironment

Our in vitro profiling of reduced inflammatory cytokines and increased chemokines after ERK5 depletion or inhibition was supported by pathway analysis of the TCGA pan-cancer in association with ERK5 expression. To gain clearer insight, we investigated the correlation between the estimated proportions of tumor-infiltrating immune cells in the TCGA dataset (Table S2) and the expression of total ERK5 and its isoforms. Indeed, total ERK5 expression, the expression of isoform-1 or isoform-3, and the co-expression of isoforms 1 and 3 correlated negatively with the proportion of CD8+ T-cells, CD4+ memory activated T-cells, gamma delta T-cells (**Figure 4A**, Table S6). This pattern is typical for

Citation: Mariska Miranda, Oishee Chatterjee, Esdy Rozali, Sujitha Jeya, Sarra Mestiri, Mariam Al-Muftah and Fares Al-Ejeh. ERK5 Mediates Metastatic Colonization and Remodeling of The Tumor and Tumor-Immune Microenvironment and Immunotherapy Response. Fortune Journal of Health Sciences. 8 (2025): 491-502.

Miranda M, et al., Fortune J Health Sci 2025
DOI:10.26502/fjhs.299

an immunosuppressed tumor immune microenvironment (TIME) generally and has been reported for TNBC specifically (12). Overall, higher expression of total ERK5 and isoforms 1 and 3 correlated with a suppressive TIME. This included (**a**) the inflammatory cytokines profiles observed in our profiling; (**b**) the association with immune suppressive pathways in the TCGA pan-cancer datasets mentioned earlier; (**c**) the role of ERK5 isoforms in EMT reported in our previous study (8) and that EMT is linked to immune evasive phenotype and poorer response to immunotherapy (13); and (**d**) the pattern of immune cell infiltrates in the TCGA pan-cancer tumors according to ERK5 expression (**Figure 4A**). This led us to stain the control and *ERK5*-depeleted tumors in the immune competent 4T1.2 TNBC mouse model for CD8 and CD4 T-cells. As shown in the images and the quantification in **Figure 4B**, there was a significant increase in tumor-infiltrating CD8 and CD4 T-cells in *ERK5*-depleted tumors compared to controls. This provided direct evidence for the role of ERK5 in modulating the tumor immune microenvironment. Despite the increased infiltration of CD8 and CD4 T-cells in ERK5 depleted 4T1.2 tumors, those tumors grew in the mammary fat pads similarly to controls (shNTC) as reported previously (8). Thus, the increased T-cell infiltration may not be sufficient to illicit an immune response, but *ERK5*-depletion could still improve response to immune checkpoint blockade. We then tested whether ERK5-depletion affects PD-L1 expression and improves response to anti-PD1 immunotherapy in the 4T1.2 tumor model. ERK5-depletion significantly reduced PD-L1 (**Figure 5A**) and enhanced sensitivity to anti-PD1 therapy, with reduced tumor growth and prolonged survival where 80% of mice remaining tumor-free to 42 days post treatment (**Figure 5B-D**).

Discussion

This study builds on our prior identification of a mechanism regulating the subcellular localization of active ERK5 (pERK5) by a truncated ERK5 isoform (isoform-3). Specifically, the retention of pERK5 outside the nucleus promoted EMT, cytoplasmic signaling, and therapeutic resistance (8). Here, we demonstrate that ERK5 knockdown using independent shRNAs significantly reduces metastatic colonization in the lung. We show that loss of ERK5 impairs the early survival of disseminated cells in vivo as evidenced by reduced proliferation and increased apoptosis in lung

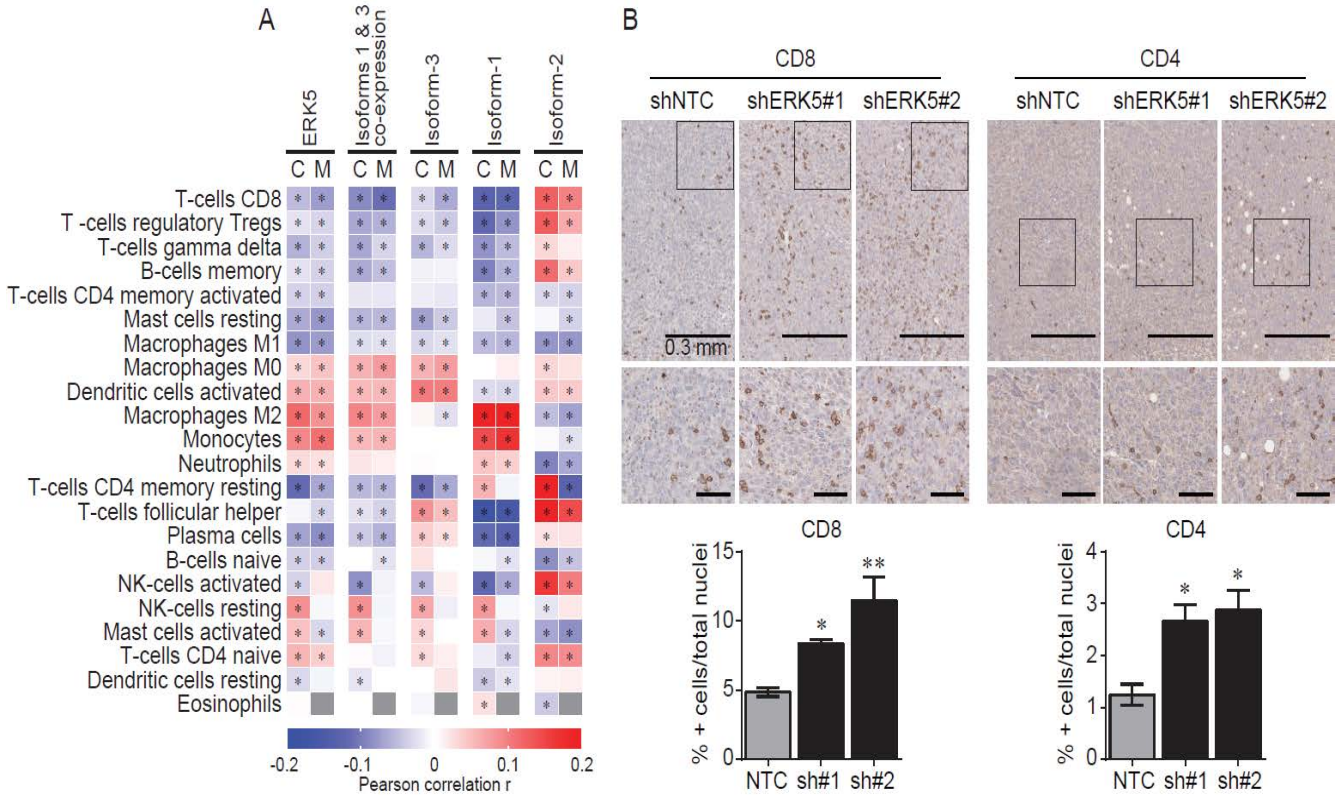

Figure 4: ERK5 modulates the tumor immune microenvironment. (**A**) The proportion of immune cell types based on two RNA-seq deconvolution methods, CIBERSORT (C) and MIXTURE (M) for the TCGA pan-cancer cases was correlated with the expression of ERK5 and its isoforms. Refer to Table S2 for the original data and Table S6 for the Pearson correlation r data depicted in the heatmap. (**B**) Control (shNTC) and ERK5-depleted 4T1.2 tumors were stained for CD8 and CD4. Images shown are at 8x magnification (scale bar = 0.3 mm) and zoomed images (scale bar = 100 mm). Bar graphs summarize the quantification (mean ± SEM, n = 3) using IHC Profiler (* P<0.05, ** P<0.01, one-way ANOVA).

Citation: Mariska Miranda, Oishee Chatterjee, Esdy Rozali, Sujitha Jeya, Sarra Mestiri, Mariam Al-Muftah and Fares Al-Ejeh. ERK5 Mediates Metastatic Colonization and Remodeling of The Tumor and Tumor-Immune Microenvironment and Immunotherapy Response. Fortune Journal of Health Sciences. 8 (2025): 491-502.

Miranda M, et al., Fortune J Health Sci 2025
DOI:10.26502/fjhs.299

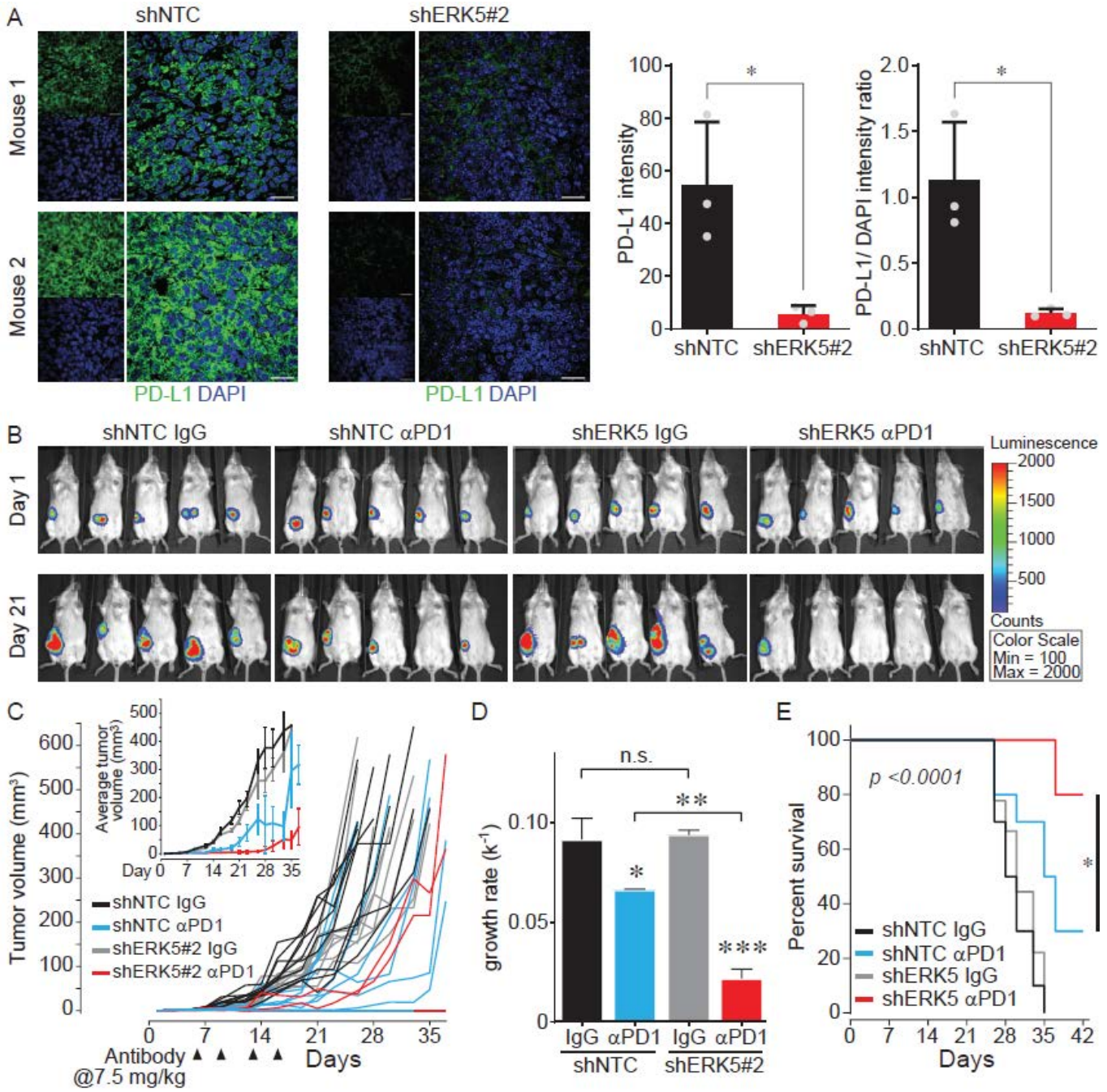

Figure 5: ERK5 depletion potentiates immunotherapy response in vivo. (**A**) Control and *ERK5*-depleted 4T1.2 tumors were compared for the expression of PD-L1. Images are shown from two independent mice from the two groups for PD-L1 expression (green) against nuclei (DAPI, blue). Scale bar = 10 mm. The intensity of PD-L1 staining and the ratio of PD-L1 intensity to DAPI intensity are summarized in the bar graphs (n=3). * $P < 0.05$ (*t*-test, GraphPad Prism). (**B-E**) Balb/c mice were injected in the mammary fat pads with control (shNTC) or *ERK5*-depleted (shERK5#2) 4T.1 cells and imaged on the next day (day 1) and weekly thereafter. Those mice were treated with anti-mouse PD1 antibody or control IgG (7.5 mg/kg) on days 6, 9, 13 and 16. Tumor growth was tracked using caliper measurements until tumors reached 500 mm^3 in size or on day 42. This immunotherapy was carried out twice with 5 mice per group in each replication (n = 10 in total). Mouse imaging in panel B is shown from one experiment. Individual tumor growth in panel C and the average (± SEM) shown in the inset graph are from all 10 mice in the experiment. The growth rates were calculated with GraphPad using exponential growth equation and shown as average (± SEM, n = 10) growth rate (k-1) in panel D. * $P < 0.05$, ** $P < 0.01$, *** $P < 0.001$ from one-way anova comparison with the control group (shNTC treated with control IgG). The survival of mice (n = 10 per group) is shown in panel E based on the end point of 500 mm^3 maximum tumor size before animal sacrifice. There was no toxicity or significant weight loss in mice in any of the groups (Data not shown).

Citation: Mariska Miranda, Oishee Chatterjee, Esdy Rozali, Sujitha Jeya, Sarra Mestiri, Mariam Al-Muftah and Fares Al-Ejeh. ERK5 Mediates Metastatic Colonization and Remodeling of The Tumor and Tumor-Immune Microenvironment and Immunotherapy Response. Fortune Journal of Health Sciences. 8 (2025): 491-502.

Miranda M, et al., Fortune J Health Sci 2025
DOI:10.26502/fjhs.299

lesions. These findings support a role for ERK5 in metastatic outgrowth and survival at secondary sites, possibly through pathways beyond canonical nuclear transcriptional regulation. Mechanistically, our proteomic and transcriptomic profiling revealed that ERK5 depletion leads to a broad downregulation of extracellular matrix (ECM) degradation and remodeling, cytokines, and growth factor receptor signaling pathways. This includes the suppression of key mesenchymal regulators and signaling nodes such as integrins, matrix metalloproteinases (MMPs), and inflammatory mediators. The role of ERK5 in EMT had conflicting reports (14-22) but our study supports a positive involvement of ERK5 in EMT. Our results linking ERK5 with ECM remodeling are supported by previous studies (23). Our findings are also in line with previous studies connecting ERK5 with inflammatory cytokines (24, 25). Beyond the agreement of our findings with previous studies on ERK5, our gene network analysis confirmed a coordinated loss of ECM-related and immune-modulatory signaling pathways. This reinforces the hypothesis that ERK5 may not only regulate intrinsic tumor cell behavior but also the microenvironmental context that supports metastasis. This was studied in the clinical context using gene programs and ssGSEA pathways in the TCGA pan-cancer datasets where we found that tumors with high co-expression of ERK5 isoform-1 and isoform-3 were significantly enriched for EMT, ECM, and cytokine signaling programs. These correlations support the mechanistic observations from our cell line and in vivo models to suggest that isoform-specific ERK5 signaling contributes to the mesenchymal transcriptional landscape in clinical tumors.

We next explored the immunological consequences of ERK5 modulation. Immune deconvolution using both CIBERSORT and MIXTURE revealed that tumors with high isoform-1/3 co-expression were significantly depleted in CD8+ T cells and enriched in immune-suppressive phenotypes. This immune exclusion signature is consistent with poor infiltration of effector T cells and suggests a mechanism of immune evasion downstream of ERK5 signaling. Furthermore, immunofluorescence of *ERK5*-depleted tumors revealed decreased PD-L1 expression and enhanced CD8+ T cell infiltration, reinforcing a functional link between ERK5 activity and the tumor immune microenvironment. An increase in T-cell infiltration after *ERK5* deletion was previously reported in a mouse model of prostate cancer (26). Mechanisms controlling PD-L1 expression in cancer involving pathways we identified in our profiling have been reviewed previously including growth factor signaling (e.g. EGF) and cytokine signaling (e.g. IL-6) through MAPK, PI3K/AKT, and STAT pathways (27). Although the expression of ERK5 and PD-L1 have been correlated previously in colorectal cancer cells (28), our study provides a direct link for ERK5 and PD-L1 expression.

The immune alterations we observed in vitro and in vivo translated into functional consequences: *ERK5* knockdown significantly enhanced the response to anti-PD1 therapy in vivo. Tumors with reduced *ERK5* expression exhibited delayed growth and prolonged survival following immune checkpoint blockade. These results support a model in which ERK5 sustains an immune-suppressive, ECM-rich tumor environment that hinders immune infiltration and contributes to checkpoint resistance. To our knowledge, this is the first report on the role of ERK5 in the response to immune checkpoint blockade. MEK inhibitors which target the activation of ERK1 and ERK2 by MEK1 and MEK2 have been shown previously to potentiate anti-PD1 immunotherapy in mice (29). In humans, triplet combination of BRAF/MEK inhibitors with immune checkpoint inhibitors in melanoma has been trialed (30, 31). Our results show that ERK5 might be an alternative MAPK pathway that should be considered for combination with immunotherapy because ERK5 is activated by MEK5, a kinase not targeted by the current MEK inhibitors used clinically.

Several limitations should be considered in our study. The temporal dynamics of ERK5 isoform switching during disease progression and therapy response are not yet understood. Second, while immune deconvolution and in vivo response data suggest that ERK5 modulates immune escape, mechanistic dissection of how ERK5 interfaces with specific cytokine-receptor interactions and antigen presentation pathways is warranted. Third, current small molecule inhibitors against ERK5 are not potent or selective to consider for testing ERK5 inhibition with immune checkpoint inhibition. Finally, and more importantly, our results with *ERK5* depletion by shRNA to achieve better response to anti-PD1 therapy do not dissect whether the response mechanism depended on targeting a specific isoform such as isoform-3, inhibiting the general activation of ERK5, or preventing the localization of pERK5 in the cytoplasm. In conclusion, we demonstrate that ERK5 expression, particularly high co-expression of isoforms 1 and 3, supports metastasis, ECM remodeling, immune suppression, and resistance to immune checkpoint blockade. Our findings highlight the need for isoform-aware targeting strategies and establish ERK5 as a critical modulator of tumor-stroma-immune interactions. As interest in the tumor immune microenvironment continues to expand, isoform-specific regulators like ERK5 offer promising avenues for improving therapeutic precision in aggressive cancers.

Methods

Breast cancer cell culture

The MDA-MB-231 cells were obtained from ATCC™ were cultured as per ATCC™ instructions, tested for mycoplasma and authenticated using STR profiling. 4T1.2

Miranda M, et al., Fortune J Health Sci 2025
DOI:10.26502/fjhs.299

cells were gifted by Dr Cameron Johnstone (Monash University, Melbourne, Australia). The generation of stable MDA-MB-231 and 4T1.2 cell lines with non-target control shRNA (shNTC) or ERK5 shRNAs were described earlier (8). For reference here, the IDs for the *ERK5* shRNAs used were: TRCN0000001356 and TRCN0000010262 for human, TRCN0000023236 and TRCN0000232396 for mouse.

In vivo models

The QIMR Berghofer animal ethics committee gave approval for mouse experiments in this study. For orthotopic models, female NOD/SCID or balb/c nude mice at 5 weeks of age (Animal Resources Centre, Perth, Australia) were inoculated in the mammary fat-pads with MDA-MB-231 cells ($5x10^6$ per fat pad) or 4T1.2 cells ($1x10^6$ per fat pad) in 50 µL of 50:50 (v/v) PBS:Matrigel™ (BD Biosciences, San Jose, CA, USA). Tumor growth was measured twice weekly by calliper measurements and weekly bioluminescent imaging (125 mg/kg luciferin I.P.) with the Xenogen IVIS system (Perkin Elmer, Waltham, MA, USA). For the experimental metastasis models we used tail vein injections of $0.5x10^6$ MDA-MB-231-luc cells, suspended in sterile PBS, into 5-week-old NOD/SCID mice. Mice were monitored by bioluminescence imaging and lungs were collected at times specified in Figures and analyzed by immunohistochemistry (IHC). For the immunotherapy model, 4T1.2 cells ($1x10^6$ per fat pad) in 50 µL of 50:50 (v/v) PBS:Matrigel™ were inoculated in the mammary fat-pads of immunocompetent NOD/SCID mice. Mice bearing ERK5-depleted or control shRNA 4T1.2 tumors were treated with 7.5 mg/kg of anti-PD1 (clone 29F.1A12™, #BE0273 BioxCell, Lebanon, NH, USA) or 7.5 mg/kg of isotype control (clone 2A3, #BE0089 BioxCell) on days 6, 9, 13 and 16. Tumor growth was measured twice weekly by caliper measurements and weekly bioluminescent imaging.

Ex vivo histology and IHC

Formalin-fixed, paraffin-embedded (FFPE) tumors/lungs were used for standard H&E, Sirius Red staining for collagen (Sigma), CD8 (clone YTS 169AG 101HL, Invitrogen, Carlsbad, CA, USA), and CD4 (clone RM4-5, Invitrogen), and. IHC was performed to detect metastases using anti-Vimentin (V9, DAKO; Santa Clara, CA, USA) mAb, Ki67 (MIB-1, DAKO) or apoptosis using ApopTag® Peroxidase In Situ Apoptosis Detection Kit (Millipore, Burlington, MA, USA) as per manufacturer instructions. For IHC quantification, images of ten random regions from each tumor section were analyzed using ImageJ (V1.46d, NIH) with IHC Profiler plugin (32). Standard Tyramide Signal Amplification (TSA) protocol (Perkin Elmer) was used for PD-L1 staining (clone 10F.9G2, BioLegand, San Diego, CA, USA). Briefly, antigen retrieval was done using Dako pH 9.0 buffer for 15 min, followed by Sniper/BSA blocking for 10 min then incubated with the primary antibody 1:1000 in Da Vinci Green diluent for 30 min before MACH2 secondary for 15 min and finally with TSA Opal 520 for 10 min. Slides were counterstained with 4′,6′-diamidino-2-phenylindole (DAPI) and mounted for imaging using the Zeiss AxioSkop2 (Zeiss, Oberkochen, Germany). CellProfiler (33) was used to determine the fluorescence intensity of PD-L1 and for nuclei (based on DAPI).

Cell migration assays

Real time migration assays were performed using the xCELLigence system (CIM-Plate®; ACEA Biosciences Inc, San Diego, CA, USA) with control (shNTC) and *ERK5*-depeleted 4T1.2 cells in the absence or presence of growth factors (200 ng/mL EGF, 100 ng/mL TNF or 100 ng/mL TGF from PeproTech®) and in the absence or presence of 2 µM of the ERK5 inhibitor XMD8-92 (Selleck Chemicals, Houston, TX, USA). The conventional Transwell® Boyden chambers (Corning Inc, Corning, NY, USA) with 8 µm pore inserts used $2x10^5$ MDA-MB-231 or 4T1.2 cells which were seeded on top of the Transwell® inserts in media and placed into a 24-well cell culture dish. Similar conditions of growth factors and the ERK5 inhibitor described for the real-time migration assays were used. Cells were incubated in the Transwell® plate at 37°C for 18 hours after which non-migrating cells were removed from the upper surface of the insert. The cells were then fixed in ice-cold methanol for 20 mins and stained with Crystal violet (0.5% w/v in 25% methanol v/v) for 15 mins at RT. Excess stain was washed off and images of the membrane containing invaded cells were photographed with the Leica Inverted DMIRB microscope (Leica, Wetzlar, Germany) with a Nikon Fi1c camera and Nikon NIS Elements software version 4.0.

Profiling assays

For the Proteome Profiler™ arrays, lysates from cell lines were hybridized to the arrays and phosphorylation levels were detected and quantified as per manufacturer instructions (R&D Systems, Minneapolis, MI, USA). The nanoString PanCancer Pathways assays were carried out using 50 ng of total RNA (nanoString® Technologies, Seattle, WA, USA) as described previously (34). Matrix metalloprotease (MMP) activity in the conditioned media of control, *ERK5*-depleted or XMD8-92 treated MDA231 cells was assayed over 4 hours using the OMNIMMP® fluorogenic substrate (Enzo Life Sciences, Farmingdale, NY, USA). Briefly, 5 µL of sample was added to 195 µL of substrate (4mM) in 96-well plates, then fluorescence was measured using a microplate reader (328 nm excitation, 393 nm emission).

TCGA transcript specific expression analysis

The expression of ERK5 isoforms in the TCGA pan-

cancer dataset was reported in our previous study (cite first paper). Briefly, the pan-cancer TCGA RNA-seq data (transcript expression TOIL RSEM FPKM) was obtained using the UCSC Xena platform (http://xena.ucsc.edu/) and the expression of ERK5 isoforms was extracted. Here, we supplemented this table (**Table S2**) the following data from the Xena platform:

Gene expression (RNA-seq) of the 175 RNAs and proteins we identified from profiling MDA-MB-231 cells with ERK5 depletion or inhibition.

Gene programs and canonical pathways (collectively called GPs) (9)

Pathway activity - z score of 1378 constituent PARADIGM pathways as single sample gene set enrichment analysis (ssGSEA) (10)

Table S2 was also supplemented with published estimations of the proportion of different types of infiltrating immune cells using two RNA-seq deconvolution methods applied to the TCGA pan-cancer data; CIBERSORT (12) and MIXTURE (11). The RNA expression of *ERK5* and *ERK5* isoforms was then correlated using Pearson correlation (GraphPad Prism) to report the correlation coefficient (r) and the significance of the correlation (two-tailed p-value) with each of (**a**) the expression of the 175 RNAs we identified in vitro (**Table S3**), (**b**) the activation scores for the GPs (**Table S4**), (**c**) the pathway activity score for the 1378 ssGSEA (**Table S5**), and (**d**) the estimated proportions of tumor-infiltrating immune cells using the two RNA-seq deconvolution methods (**Table S6**).

Statistical analysis

All statistical analysis was performed using GraphPad Prism® (v.7, GraphPad Software). The types of tests performed are indicated in respective Figure legends.

Conflict of Interest

The authors declare that they have no competing interests.

Author Contributions

M.M. and F.A. designed the experimental plan, coordinated the collaborations, and data analyses. M.M. executed most of the experiments, including the cell culture and lentiviral production, *in vivo* models, immunofluorescence, Proteome Profiler arrays, RT-PCR arrays and validation, scratch wound and Transwell migration assays. xCELLigence assays for cell migration and optimisation of OMNIMMP® fluorogenic substrate assays were done by O.C. S.J, S.M, M.A. and F.A. designed and executed the bioinformatics analysis relating to ERK5 and ERK5 isoforms and pathways in the TCGA pan-cancer dataset. M.M, and F.A. wrote the paper with input from all other authors. Funding acquisition by F.A.

Funding

This research was funded by the Cancer Council Queensland, APP1106310 to F.A. F.A. was supported by Australian Research Council Fellowship (FT130101417). M.M, O.C, and E.N.R. were supported by the Australian National Health and Medical Research Council (NHMRC Grant APP1082458 to F.A.). F.A, S.J, S.M. and M.A. are supported by Qatar Biomedical Research Institute (QBRI) Funding. Publication Open Access charges were supported by QBRI (IGP5 grant to F.A.).

Acknowledgments

We thank the QIMR Berghofer Flow cytometry, Microscopy and Histology facilities for technical support.

References

1. Bray F, Laversanne M, Sung H, et al. Global cancer statistics 2022: GLOBOCAN estimates of incidence and mortality worldwide for 36 cancers in 185 countries. CA Cancer J Clin 74 (2024): 229-263.
2. Lee J. Current Treatment Landscape for Early Triple-Negative Breast Cancer (TNBC). J Clin Med 12 (2023).
3. Yin L, Duan JJ, Bian XW, et al. Triple-negative breast cancer molecular subtyping and treatment progress. Breast Cancer Res 22 (2020): 61.
4. Derakhshan F and Reis-Filho JS. Pathogenesis of Triple-Negative Breast Cancer. Annu Rev Pathol 17 (2022): 181-204.
5. Bianchini G, Balko JM, Mayer IA, et al. Triple-negative breast cancer: challenges and opportunities of a heterogeneous disease. Nat Rev Clin Oncol 13 (2016): 674-690.
6. Stecca B and Rovida E. Impact of ERK5 on the Hallmarks of Cancer. Int J Mol Sci 20 (2019).
7. Monti M, Celli J, Missale F, et al. Clinical Significance and Regulation of ERK5 Expression and Function in Cancer. Cancers (Basel) 14 (2022).
8. Miranda M, Saunus JM, Akgül S, Moradi Marjaneh M, et al. A Short ERK5 Isoform Modulates Nucleocytoplasmic Shuttling of Active ERK5 and Associates with Poor Survival in Breast Cancer. Fortune Journal of Health Sciences 8 (2025): 250-266.
9. Hoadley KA, Yau C, Hinoue T, Wolf DM, et al. Cell-of-Origin Patterns Dominate the Molecular Classification of 10,000 Tumors from 33 Types of Cancer. Cell 173 (2018): 291-304.
10. Newman AM, Liu CL, Green MR, Gentles AJ, et al.

Robust enumeration of cell subsets from tissue expression profiles. Nat Methods 12 (2015): 453-7.

11. Fernandez EA, Mahmoud YD, Veigas F, Rocha D, et al. Unveiling the immune infiltrate modulation in cancer and response to immunotherapy by MIXTURE-an enhanced deconvolution method. Brief Bioinform 22 (2021).
12. Craven KE, Gokmen-Polar Y and Badve SS. CIBERSORT analysis of TCGA and METABRIC identifies subgroups with better outcomes in triple negative breast cancer. Sci Rep 11 (2021): 4691.
13. Wang G, Xu D, Zhang Z, Li X, et al. The pan-cancer landscape of crosstalk between epithelial-mesenchymal transition and immune evasion relevant to prognosis and immunotherapy response. NPJ Precis Oncol 5 (2021): 56.
14. Zhou C, Nitschke AM, Xiong W, Zhang Q, et al. Proteomic analysis of tumor necrosis factor-alpha resistant human breast cancer cells reveals a MEK5/Erk5-mediated epithelial-mesenchymal transition phenotype. Breast Cancer Res 10 (2008): R105.
15. Javaid S, Zhang J, Smolen GA, Yu M, et al. MAPK7 Regulates EMT Features and Modulates the Generation of CTCs. Mol Cancer Res 13 (2015): 934-43.
16. Liu F, Zhang H and Song H. Upregulation of MEK5 by Stat3 promotes breast cancer cell invasion and metastasis. Oncol Rep 37 (2017): 83-90.
17. Morikawa M, Koinuma D, Mizutani A, Kawasaki N, et al. BMP Sustains Embryonic Stem Cell Self-Renewal through Distinct Functions of Different Kruppel-like Factors. Stem Cell Reports 6 (2016): 64-73.
18. Chen R, Yang Q and Lee JD. BMK1 kinase suppresses epithelial-mesenchymal transition through the Akt/GSK3beta signaling pathway. Cancer Res 72 (2012): 1579-87.
19. Liang Z, Xie W, Wu R, Geng H, et al. ERK5 negatively regulates tobacco smoke-induced pulmonary epithelial-mesenchymal transition Oncotarget 6 (2015): 19605-18.
20. Pavan S, Meyer-Schaller N, Diepenbruck M, Kalathur RKR, et al. A kinome-wide high-content siRNA screen identifies MEK5-ERK5 signaling as critical for breast cancer cell EMT and metastasis. Oncogene (2018).
21. Zhai L, Ma C, Li W, Yang S, et al. miR-143 suppresses epithelial-mesenchymal transition and inhibits tumor growth of breast cancer through down-regulation of ERK5. Mol Carcinog 55 (2016): 1990-2000.
22. Bhatt AB, Patel S, Matossian MD, Ucar DA, et al. Molecular Mechanisms of Epithelial to Mesenchymal Transition Regulated by ERK5 Signaling. Biomolecules 11 (2021).
23. Hoang VT, Matossian MD, Ucar DA, Elliott S, et al. ERK5 Is Required for Tumor Growth and Maintenance Through Regulation of the Extracellular Matrix in Triple Negative Breast Cancer. Front Oncol 10 (2020): 1164.
24. Wilhelmsen K, Mesa KR, Lucero J, Xu F, et al. ERK5 protein promotes, whereas MEK1 protein differentially regulates, the Toll-like receptor 2 protein-dependent activation of human endothelial cells and monocytes. J Biol Chem 287 (2012): 26478-94.
25. Finegan KG, Perez-Madrigal D, Hitchin JR, et al. ERK5 is a critical mediator of inflammation-driven cancer. Cancer Res 75 (2015): 742-53.
26. Loveridge CJ, Mui EJ, Patel R, Tan EH, et al. Increased T-cell Infiltration Elicited by Erk5 Deletion in a Pten-Deficient Mouse Model of Prostate Carcinogenesis. Cancer Res 77 (2017): 3158-3168.
27. Cha JH, Chan LC, Li CW, Hsu JL, et al. Mechanisms Controlling PD-L1 Expression in Cancer. Mol Cell 76 (2019): 359-370.
28. Zhang M, Shi R, Guo Z, and He J. Cancer-associated fibroblasts promote cell growth by activating ERK5/PD-L1 signaling axis in colorectal cancer. Pathol Res Pract 216 (2020): 152884.
29. Ebert PJR, Cheung J, Yang Y, McNamara E, et al. MAP Kinase Inhibition Promotes T Cell and Anti-tumor Activity in Combination with PD-L1 Checkpoint Blockade. Immunity 44 (2016): 609-621.
30. Dixon-Douglas JR, Patel RP, Somasundram PM and McArthur GA. Triplet Therapy in Melanoma - Combined BRAF/MEK Inhibitors and Anti-PD-(L)1 Antibodies. Curr Oncol Rep 24 (2022): 1071-1079.
31. Dummer R, Welti M and Ramelyte E. The role of triple therapy and therapy sequence in treatment of BRAF-mutant metastatic melanoma. Response to overall survival with first-line atezolizumab in combination with vemurafenib and cobimetinib in BRAFV600 mutation-positive advanced melanoma (IMspire150): second interim analysis of a multicentre, randomised, phase 3 study. J Transl Med 21 (2023): 529.
32. Varghese F, Bukhari AB, Malhotra R and De A. IHC Profiler: an open-source plugin for the quantitative evaluation and automated scoring of immunohistochemistry images of human tissue samples 9 (2014): e96801.
33. Carpenter AE, Jones TR, Lamprecht MR, Clarke C, et al. CellProfiler: image analysis software for identifying

and quantifying cell phenotypes. Genome Biol 7 (2006): R100.

34. Johnson J, Bessette DC, Saunus JM, Smart CE, et al. Characterization of a novel breast cancer cell line derived from a metastatic bone lesion of a breast cancer patient. Breast Cancer Res Treat 170 (2018): 179-188.

Citation: Mariska Miranda, Oishee Chatterjee, Esdy Rozali, Sujitha Jeya, Sarra Mestiri, Mariam Al-Muftah and Fares Al-Ejeh. ERK5 Mediates Metastatic Colonization and Remodeling of The Tumor and Tumor-Immune Microenvironment and Immunotherapy Response. Fortune Journal of Health Sciences. 8 (2025): 491-502.